Research Article | Vol. 26, No. 7 | 2 Apr 2018 | OPTICS EXPRESS 8385
Optics EXPRESS

Topographically induced homeotropic alignment of liquid crystals on self-assembled opal crystals

PANKAJ KUMAR,[1,2] SU YEON OH,[1] VIJAY K. BALIYAN,[1] SUDARSHAN KUNDU,[1] SEUNG HEE LEE,[1,3] AND SHIN-WOONG KANG[1,4]

[1]*Department of BIN Convergence Technology, Chonbuk National University, Jeonju 54896, South Korea*
[2]*Chitkara University Research and Innovation Network & Department of Applied Sciences, Chitkara University, Patiala (Punjab) 140401, India*
[3]*lsh1@jbnu.ac.kr*
[4]*swkang@jbnu.ac.kr*

Abstract: The surface of multilayered opal crystals resulted in homeotropic alignment of liquid crystal (LC), originated from the surface topography of opal crystals rather than a chemical nature of the nanoparticles. The polar anchoring energy (5.51×10^{-5} J/m^2) of the crystal surface for nematic LC molecules was in a similar range to the conventional polyimide alignment layer (2.11×10^{-5} J/m^2) used for commercial applications. The critical length scale for anchoring transition was approximately L_w = ~1 μm. If a diameter of particle d << 1 μm for opal crystals, LC molecules preferred to anchor vertically to the surface to minimize elastic free energy of bulk LCs. The LC favored a planar anchoring if d >> 1 μm. The results provide crucial insights to understand the homeotropic alignment of LCs on solid surfaces and therefore offer opportunities to develop novel materials for a vertical alignment of LCs.

OCIS codes: (230.3720) Liquid-crystal devices; (160.3710) Liquid crystals.

References and links

1. K. Takatoh, M. Hasegawa, M. Koden, N. Otoh, R. Hasegawa, and M. Sakamoto, *Alignment Technologies and Applications of Liquid Crystal Devices* (Taylor and Francis, 2005) Chaps. 2 and 3.
2. J. L. Janning, "Thin film surface orientation for liquid crystals," Appl. Phys. Lett. **21**(4), 173–174 (1972).
3. M. Lu, "Liquid crystal orientation induced by Van der walls interaction," Jpn. J. Appl. Phys. **43**(12), 8156–8160 (2004).
4. W. M. Gibbons, P. J. Shannon, S. Sun, and B. J. Swetlin, "Surface-mediated alignment of nematic liquid crystals with polarized laser light," Nature **351**(6321), 49–50 (1991).
5. Y. Wu, Y. Demachi, O. Tsutsumi, A. Kanazawa, T. Shiono, and T. Ikeda, "Photoinduced alignment of polymer liquid crystals containing azobenzene moieties in the side chain. 1. Effect of light intensity on alignment behavior," Macromolecules **31**(2), 349–354 (1998).
6. D. S. Seo, S. Kobayashi, D. Y. Kang, and H. Yokoyama, "Effects of rubbing and temperature dependence of polar anchoring strength of homogeneously aligned nematic liquid crystal on polyimide langmuir-blodgett orientation films," Jpn. J. Appl. Phys. **34**(1), 3607–3611 (1995).
7. P. Chaudhari, J. Lacey, J. Doyle, E. Galligan, S. C. A. Lien, A. Callegari, G. Hougham, N. D. Lang, P. S. Andry, R. John, K. H. Yang, M. Lu, C. Cai, J. Speidell, S. Purushothaman, J. Ritsko, M. Samant, J. Stöhr, Y. Nakagawa, Y. Katoh, Y. Saitoh, K. Sakai, H. Satoh, S. Odahara, H. Nakano, J. Nakagaki, and Y. Shiota, "Atomic-beam alignment of inorganic materials for liquid-crystal displays," Nature **411**(6833), 56–59 (2001).
8. J. P. Doyle, P. Chaudhari, J. L. Lacey, E. A. Galligan, S. C. Lien, A. C. Callegari, N. D. Lang, M. Lu, Y. Nakagawa, H. Nakano, N. Okazaki, S. Odahara, Y. Katoh, Y. Saitoh, K. Sakai, H. Satoh, and Y. Shiota, "Ion beam alignment for liquid crystal display fabrication," Nucl. Instrum. Methods Phys. Res. B **206**, 467–471 (2003).
9. J. S. Gwag, C. G. Jhun, J. C. Kim, T. H. Yoon, G. D. Lee, and S. J. Cho, "Alignment of liquid crystal on a polyimide surface exposed to an Ar ion beam," J. Appl. Phys. **96**(1), 257–260 (2004).
10. J. Stöhr, M. G. Samant, J. Luning, A. C. Callegari, P. Chaudhari, J. P. Doyle, J. A. Lacey, S. A. Lien, S. Purushothaman, and J. L. Speidell, "Liquid crystal alignment on carbonaceous surfaces with orientational order," Science **292**(5525), 2299–2302 (2001).
11. P. K. Son, J. H. Park, J. C. Kim, and T. H. Yoon, "Control of liquid crystal alignment by deposition of silicon oxide thin film," Thin Solid Films **515**(5), 3102–3106 (2007).

#323015 https://doi.org/10.1364/OE.26.008385
Journal © 2018 Received 12 Feb 2018; revised 9 Mar 2018; accepted 13 Mar 2018; published 22 Mar 2018

Optics EXPRESS

12. W. Y. Chou, Z. Y. Ho, F. C. Tang, Y. S. Mai, T. Y. Wu, H. L. Cheng, C. R. Sheu, C. C. Liao, and K. H. Liu, "Ion-beam-processed SiO_2 film for homogeneous liquid crystal alignment," Jpn. J. Appl. Phys. **44**(27 6L), L876–L878 (2005).
13. P. K. Son, J. H. Park, J. C. Kim, T. H. Yoon, S. J. Rho, B. K. Jeon, S. T. Shin, J. S. Kim, and S. K. Lim, "Vertical alignment of liquid crystal through ion beam exposure on oxygen-doped SiC films deposited at room temperature," Appl. Phys. Lett. **91**(10), 103513 (2007).
14. H. C. Moon, H. K. Kang, J. Y. Hwang, Y. P. Park, S. H. Lim, J. Jang, and D.-S. Seo, "Vertical alignment of nematic liquid crystal by rubbing-free method on the SiC thin film layer," Jpn. J. Appl. Phys. **45**(1), 7017–7019 (2006).
15. S. K. Lee, J. H. Kim, B. Y. Oh, D. H. Kang, B. Y. Kim, J. W. Han, Y. H. Kim, J. M. Han, J. Y. Hwang, C. H. Ok, and D. S. Seo, "Liquid crystal alignment effects on SiN_x thin film layers treated by ion-beam irradiation," Jpn. J. Appl. Phys. **46**(12), 7711–7713 (2007).
16. C. Chen, J. E. Anderson, and P. J. Bos, "Uniform vertical alignment of a liquid crystal that has a large negative dielectric," Jpn. J. Appl. Phys. **44**(35), L1126–L1127 (2005).
17. C. Chen, P. J. Bos, J. Kim, Q. Li, and J. E. Anderson, "Improved liquid crystal for vertical alignment applications," J. Appl. Phys. **99**(12), 123523 (2006).
18. C. Chen, P. J. Bos, and J. E. Anderson, "Anchoring transitions of liquid crystals on SiO_x," Liq. Cryst. **35**(4), 465–481 (2008).
19. Y. Yi, G. Lombardo, N. Ashby, R. Barberi, J. E. Maclennan, and N. A. Clark, "Topographic-pattern-induced homeotropic alignment of liquid crystals," Phys. Rev. E Stat. Nonlin. Soft Matter Phys. **79**(4 Pt 1), 041701 (2009).
20. D. W. Berreman, "Solid surface shape and the alignment of an adjacent nematic liquid crystal," Phys. Rev. Lett. **28**(26), 1683–1686 (1972).
21. H. S. Jeong, H.-J. Jeon, Y. H. Kim, M. B. Oh, P. Kumar, S.-W. Kang, and H.-T. Jung, "Bifunctional ITO layer with a high resolution, surface nano-pattern for alignment and switching of LCs in device applications," NPG Asia Mater. **4**(2), e7 (2012).
22. S. Kundu, M.-H. Lee, S. H. Lee, and S. W. Kang, "In situ homeotropic alignment of nematic liquid crystals based on photoisomerization of azo-dye, physical adsorption of aggregates, and consequent topographical modification," Adv. Mater. **25**(24), 3365–3370 (2013).
23. S. Y. Oh and S. W. Kang, "Photoreactive self-assembled monolayer for the stabilization of tilt orientation of a director in vertically aligned nematic liquid crystals," Opt. Express **21**(25), 31367–31374 (2013).
24. D.-Y. Kim, S. Kim, S.-A. Lee, Y.-E. Choi, W.-J. Yoon, S.-W. Kuo, C.-H. Hsu, M. Huang, S. H. Lee, and K.-U. Jeong, "Asymmetric organic-inorganic hybrid giant molecule: cyanobiphenyl monosubstituted polyhedral oligomeric silsesquioxane nanoparticles for vertical alignment of liquid crystals," J. Phys. Chem. C **118**(12), 6300–6306 (2014).
25. Y.-F. Chung, M.-Z. Chen, S.-H. Yang, and S.-C. Jeng, "Tunable surface wettability of ZnO nanoparticle arrays for controlling the alignment of liquid crystals," ACS Appl. Mater. Interfaces **7**(18), 9619–9624 (2015).
26. S.-H. Chen, T.-R. Chou, Y.-T. Chiang, and C.-Y. Chao, "Nanoparticle-induced vertical alignment liquid crystal cell with highly conductive PEDOT: PSS films as transparent electrodes," Mol. Cryst. Liq. Cryst. (Phila. Pa.) **646**(1), 107–115 (2017).
27. J. Sun, C. J. Tang, P. Zhan, Z. L. Han, Z. S. Cao, and Z. L. Wang, "Fabrication of centimeter-sized single-domain two-dimensional colloidal crystals in a wedge-shaped cell under capillary forces," Langmuir **26**(11), 7859–7864 (2010).
28. M. Grzelczak, J. Vermant, E. M. Furst, and L. M. Liz-Marzán, "Directed self-assembly of nanoparticles," ACS Nano **4**(7), 3591–3605 (2010).
29. H. K. Choi, S. H. Im, and O. O. Park, "Fabrication of unconventional colloidal self-assembled structures," Langmuir **26**(15), 12500–12504 (2010).
30. N. Denkov, O. D. Velev, P. A. Kralchevski, I. B. Ivanov, H. Yoshimura, and K. Nagayama, "Mechanism of formation of two-dimensional crystals from latex particles on substrates," Langmuir **8**(12), 3183–3190 (1992).
31. M. Trau, D. A. Saville, and I. A. Aksay, "Field induced layering of colloidal crystals," Science **272**(5262), 706–709 (1996).
32. S. O. Lumsdon, E. W. Kaler, J. P. Williams, and O. D. Velev, "Dielectrophoretic assembly of oriented and switchable two-dimensional photonic crystals," Appl. Phys. Lett. **82**(6), 949–951 (2003).
33. K. Q. Zhang and X. Y. Liu, "In situ observation of colloidal monolayer nucleation driven by an alternating electric field," Nature **429**(6993), 739–743 (2004).
34. P. Jiang, T. Prasad, M. J. Mcfarland, and V. L. Colvin, "Two-dimensional non close-packed colloidal crystals formed by spin coating," Appl. Phys. Lett. **89**(1), 011908 (2006).
35. A. Mihi, M. Ocana, and H. Miguez, "Oriented colloidal-crystal thin films by spin-coating microspheres dispersed in volatile media," Adv. Mater. **18**(17), 2244–2249 (2006).
36. B. van Duffel, R. H. A. Ras, F. C. De Schryver, and R. A. Schoonheydt, "Langmuir–Blodgett deposition and optical diffraction of two-dimensional Opal," J. Mater. Chem. **11**(12), 3333–3336 (2001).
37. A. S. Dimitrov and K. Nagayama, "Continuous convective assembling of fine particles into two-dimensional arrays on solid surfaces," Langmuir **12**(5), 1303–1311 (1996).
38. P. Jiang, J. F. Bertone, K. S. Hwang, and V. L. Colvin, "Single-crystal colloidal multilayers of controlled thickness," Chem. Mater. **11**(8), 2132–2140 (1999).

Optics EXPRESS

39. S. Wong, V. Kitaev, and G. A. Ozin, "Colloidal crystal films: advances in universality and perfection," J. Am. Chem. Soc. **125**(50), 15589–15598 (2003).
40. S. Faetti, "Azimuthal anchoring energy of a nematic liquid crystal at a grooved interface," Phys. Rev. A Gen. Phys. **36**(1), 408–410 (1987).
41. J. Fukuda, M. Yoneya, and H. Yokoyama, "Surface-groove-induced azimuthal anchoring of a nematic liquid crystal: Berreman's model reexamined," Phys. Rev. Lett. **98**(18), 187803 (2007).
42. S. Kumar, J.-H. Kim, and Y. Shi, "What aligns liquid crystals on solid substrates? The role of surface roughness anisotropy," Phys. Rev. Lett. **94**(7), 077803 (2005).
43. L. Malaquin, T. Kraus, H. Schmid, E. Delamarche, and H. Wolf, "Controlled particle placement through convective and capillary assembly," Langmuir **23**(23), 11513–11521 (2007).
44. S. Tsuji and H. Kawaguchi, "Self-assembly of poly(N-isopropylacrylamide)-carrying microspheres into two-dimensional colloidal arrays," Langmuir **21**(6), 2434–2437 (2005).
45. V. K. Gupta and N. L. Abbott, "Design of surfaces for patterned alignment of liquid crystals on planar and curved substrates," Science **276**(5318), 1533–1536 (1997).
46. A. Pizzirusso, R. Berardi, L. Muccioli, M. Ricci, and C. Zannoni, "Predicting surface anchoring: molecular organization across a thin film of 5CB liquid crystal on Silicon," Chem. Sci. (Camb.) **3**(2), 573–579 (2012).
47. I. Drevenšek Olenik, K. Kocevar, I. Musevic, and T. Rasing, "Structure and polarity of 8CB films evaporated onto solid substrates," Eur Phys J E Soft Matter **11**(2), 169–175 (2003).
48. O. D. Lavrentovich, "Transport of particles in liquid crystals," Soft Matter **10**(9), 1264–1283 (2014).

1. Introduction

Liquid crystal (LC) is a fascinating state of matter with soft crystalline nature. On a broader sense, self-assembly of molecules with shape anisotropy constitutes the simplest liquid crystalline phase with nematic order. Soft crystalline nature with orientational order along with large optical anisotropy made nematic LC as a powerful component for electro-optical devices. Usually to make an effective device, orientation of nematic molecules needs to be controlled by electric field from external source. To yield a specific orientation of the molecules without any external field, however, an anisotropically modified surface is used. Thus a specially treated surface is a prerequisite component for electro-optic device applications [1]. The most widely adopted method for controlling the director orientation adjacent to solid surface is coating of polyimide layer on a substrate with transparent electrodes [1]. For homogenous or planar alignment, in which LC director is parallel to the substrate plane, polyimide with short or no side chain is used. In case of homeotropic or vertical alignment, where the LC director is perpendicular to the substrate, polyimide with relatively longer side chain is used. However, the use of polyimide layer has some drawbacks, such as static electric charges and debris due to mechanical rubbing, and high curing temperature, etc. Since alignment control is one of the most crucial and essential process for the fabrication of LC displays, various researches have been performed to find potential alternatives to replace polyimide.

To overcome the problem, for the alignment of LCs, the non-contact techniques such as the oblique evaporation [2,3], photo-alignment [4,5], Langmuir–Blodgett films [6] and ion-beam alignment [7–9], were proposed to resolve the drawbacks of the contact (i.e. rubbing) technique and have been a great topic of interest for last two decades. More recently, numerous inorganic materials, such as diamond like carbon [7,10], SiO_x [11,12], SiC [13,14] and SiN_x [7,15] were studied with ion-beam alignment technique and attracted much attention due to their potential for achieving good uniformity in large-sized substrates as well as having strong anchoring energy with high thermal stability, as compared with photo-alignment and oblique evaporation approaches. However, many issues related to the mechanism of alignment of LCs were not yet established, especially in the case of the vertical alignment of the LCs on the inorganic alignment layer. Not only may the chemical nature of the surface, but also its roughness cause homeotropic alignment. Lu [3] showed that the sign of dielectric anisotropy ($\Delta\varepsilon$) of the LC, rather than the columnar structure of a-SiO_x thin film, plays an important role in the final alignment of the LCs. In their report, vertical alignment was usually obtained for a LC with a negative $\Delta\varepsilon$, while planar alignment was obtained with a positive $\Delta\varepsilon$. On the other hand, Chen and associates [3,16–18] showed that the addition of material having a strong longitudinal dipole moment to a LC with large negative $\Delta\varepsilon$ brings

Optics EXPRESS

about an alignment transition from the planar to the vertical alignment. Yi, et al. [19] clearly demonstrated how a physically modified or nano-imprinted patterned substrate causes anchoring transition from planar to homeotropic alignment. Although LC molecules are prone to be planar aligned on a smooth polymer surface, once the surface is roughened causing enough elastic distortion to overcome the surface anchoring, adjacent LC medium experiences anchoring transition from planar to homeotropic state. The fact goes very well with the famous work of Berreman's theory [20] for LC anchoring on solid substrates.

In continuation, Jeong et al. [21] also described a method for vertical alignment using nano-patterns of ITO electrodes, fabricated based on the secondary sputtering phenomenon. Kundu et al. [22] demonstrated the concept of irreversible photo-stimulated anchoring transitions to a homeotropic state. Oh et al. [23] proposed an idea of vertical alignment as well as in situ stabilization of the director tilt, achieved by bifunctional photo-reactive self-assembled monolayer. Recently, Kim et al. [24] reported cyanobiphenyl substituted POSS nanoparticles for vertical alignment of LC. Chung et al. [25] demonstrated that the pretilt angle of LCs can be tuned from ~0° to ~90° using ZnO nanoparticles arrays with modified chemical property and surface wettability. Chen et al. [26] reported nanoparticle-induced vertical alignment using conductive transparent PEDOT: PSS film and illustrated the potential of flexible LC devices with high transmittance for ITO-free LC displays.

On the other hand, self-assembly of inorganic materials evidences a process by which nanoparticles spontaneously organize into ordered structure directly or indirectly, depending on their mutual interaction or an externally imposed force, respectively [27–29]. Self-assembly of such particles often yields two-dimensional (2D) mono-domain crystals over a large area. Several methods have been followed to fabricate 2D crystals such as self-assembly under capillary forces [30], electrophoretic deposition [31–33], spin casting [34,35] and Langmuir-Blodgett deposition [36], etc. Convective assembly [37–39], has been one of the most frequently used methods because of its ruggedness and minimalism. In this technique, a three-phase contact line at the meniscus of the suspension film is formed by slow evaporation liquid film and solvent thickness becomes comparable to the colloidal particle size as well as a lateral capillary force between adjacent particles drags them into contact. Gradually, evaporation and convective drag progressively free particles move toward settled colloids and lead to an entropy-favorable close packed lattice in two dimensions. This 2D assembly of NPs creates a uniform layer and can be used as an alignment controlling surface for nematic LCs.

Consequently, in present work, multilayered crystalline silica nanoparticles (i.e., opal crystal) on the ITO-glass substrate were deposited by evaporation-induced self-assembly technique and used for vertical alignment of nematic LCs. Both monodisperse and polydisperse silica nanoparticles (SNPs) were used in the separate sets of experiments to create SNPs-layers on ITO-glass substrates. Surface morphologies of the SNPs-coated substrates were studied by field emission scanning electron microscopy (FE-SEM) and atomic force microscopy (AFM). Electro-optical properties of the LC cell and polar anchoring energy of LC molecules on the SNPs-coated surface were measured and compared with the value obtained from a conventional PI-coated substrate. In our results, both crystalline layers and irregular aggregates of SNPs induced effective homeotropic anchoring of LC molecules at the surfaces. The results behind the homeotropic anchoring have been discussed based on the physical interaction with the help of Berreman's theory [20] and its further developments [40–42].

2. Experimental section

2.1. Preparation of the silica multilayer

Spherical SNPs powder having average particle diameter 15 nm (polydisperse, Nanostructured & Amorphous Materials, Inc., USA), 80 nm (polydisperse, Nanostructured & Amorphous Materials, Inc., USA) and 320 nm (monodisperse, Bangs Laboratories, Inc., USA) were purchased and used as received. Each powder was added to de-ionized water

Optics EXPRESS

separately by 0.05 ~0.2 weight percent. Homogeneous dispersions of the SNPs were obtained by stirring overnight, followed by ultrasonic process at a frequency of 20 kHz for 24 hrs at the 60°C by using sonicator (S-400 Qsonica,LLC). The mixture vials were sealed with para film to avoid evaporation of the solvents. In the experiment for the multilayer deposition, Indium-tin-oxide (ITO) coated glass plates were used as substrate. ITO-coated glass plates were cleaned in a soap solution filled sonic bath and then rinsed by deionized water, acetone and isopropyl alcohol, consecutively. The cleaned ITO-plates were kept in an oven at 120 °C for 1hr for drying. Clean and dried ITO-coated glass plates were dipped vertically in homogenous dispersions of SNPs with different sizes separately. The whole system was kept in a pre-heated chamber at 60 °C for slow evaporation of solvent. Multi-layered self-assembly of SNPs was achieved on the ITO-glass plates upon evaporation of the solvent. These SNPs coated ITO-glass substrates were used for cell fabrication to study alignment of LC molecules at the surfaces of SNPs and resulting electro-optic properties of LCs in a confined cell.

2.2. LC Cell fabrication

Multiple numbers of test cells were fabricated by using SNPs-deposited ITO-glass substrates. The cell gap of each LC cell was maintained by using tape spacers and varied according to its purpose. Some cells were fabricated with ball spacer of diameters 4.0 μm, mixed uniformly with UV-curable sealant. These cells were examined under polarizing optical microscope (POM) and used for measurements of electro-optical properties. Some other cells were fabricated using 10 and 20 μm tape spacers and used for measurements of anchoring strength of LC at SNPs-surfaces. The cells were loaded with commercially available nematic LC (Merck Performance Materials, Korea) with negative dielectric anisotropy ($\Delta\varepsilon = -4$) by capillary action at its isotropic temperature. The ordinary and extraordinary refractive indices of the LC material are 1.4742 and 1.5512, respectively. The elastic coefficients of splay and bend deformation are 13.5 pN and 15.1 pN, respectively. The nematic-to-isotropic transition temperature corresponds to 75.0 °C. For the reference homeotropic LC cell, conventional PI with no rubbing (JSR Micro Korea Co. Ltd.) was used as alignment layers.

2.3. Characterizations

To study the anchoring behaviors of LC molecules at the surface of self-assembled SNPs, the surface morphology and roughness profile of the SNPs-multilayer were examined through a field emission scanning electron microscope (FE-SEM, S4700, Hitachi, Japan) and atomic force microscopy (Agilent 550 AFM, Agilent Technologies). The optical textures and conoscopic figures were observed using a polarized optical microscope (POM, NIKON LV100POL) in order to confirm the alignment of LC molecules at the surfaces. Electro-optical properties of 4 μm cell, placed between a pair of crossed polarizers, were investigated by using the LCMS 200 (Sesim Photonics Technology). Optical retardations of the 10 μm cell were measured as a function of applied voltage across a cell, using the REMS-150 (Sesim Photonics Technology). Anchoring energy was calculated from the measured retardation values.

3. Results and discussion

For the study, a thin layer of SNPs was deposited on ITO-glass substrates by the capillary convection method. Either monodisperse or polydisperse SNPs in a colloidal dispersion self-assembled into a closely packed layer. During solvent evaporation, capillary force and convection bring particles together and form a thin uniform layer with a protruded surface [42,43]. The surfaces were characterized and used for the control of LC alignment. Fig. 1 shows structured surface morphology of the opal crystal with monodisperse 320 nm SNPs and shows resulting vertical alignment of LCs on the surface. Normal (a-i) and 20° tilted (a-ii) FE-SEM views on the surface layer corroborate closely packed crystalline order of the SNPs.

Optics EXPRESS

The AFM data in Fig. 1(b) further confirm the embossed surface with a regular hexagonal pattern.

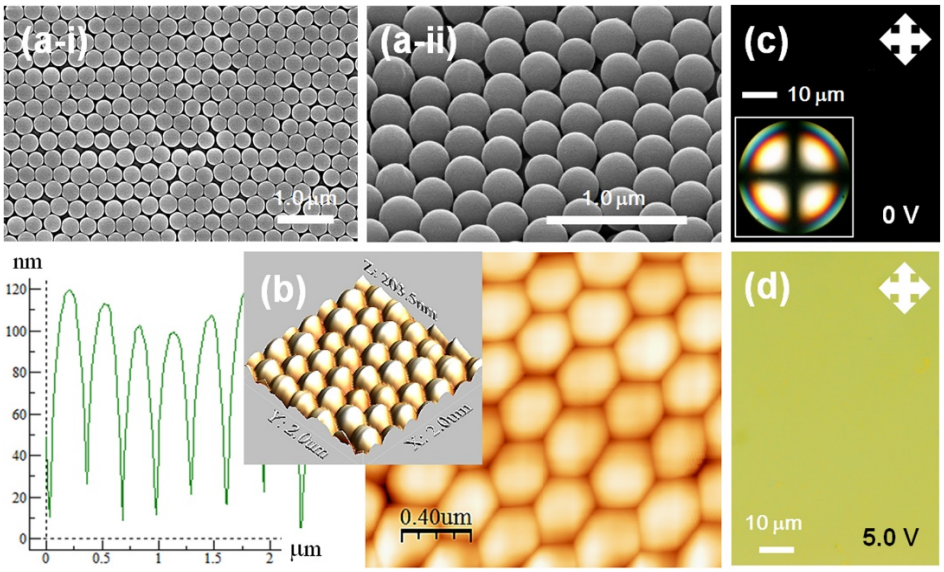

Fig. 1. Periodic surface structure of the opal crystal and electro-optical switching of the LC cell fabricated by the same: (a-i) Normal and (a-ii) tilted FE-SEM views of the surface of the opal crystal, formed by monodisperse 320 nm silica particles; (b) AFM data exemplifying regular embossed surface with a hexagonal pattern; (c) and (d) POM images of the cell at 0 V and 5.0 V, respectively. The arrows denote the transmission axes of the polarizers. The inset in (c) is the corresponding conoscopic figure.

The height profile of a surface shows regular interstitial indents at least 100 nm depth for every 320 nm. Fig. 1(c) shows the POM image of nematic LC sandwiched by the surface of opal crystals. The completely dark image with the conoscopic figure in the inset confirms a homeotropic alignment of LCs in the cell. Upon applied electric field, the texture changed to a uniform planar state at a local area as shown in Fig. 1(d). Since a director orientation in the plane of a substrate was not predetermined, azimuthal orientation of a director was not uniform in the entire cell. However, observed overall tendency was that a director reorient toward the direction of LC filling, presumably affected by a flow.

The regular crystalline order of SNPs was not a critical requirement for a homeotropic anchoring of LC molecules at the surface. Irregular stacks of SNP-aggregates also induced homeotropic alignment. Fig. 2 shows such results obtained using polydisperse SNPs with approximately 15 nm diameter. The thickness of a deposited silica layer sensitively relied on evaporation rate of a water solvent. The POM image in Fig. 2(a) exhibits two distinct regions. As shown in Fig. 2(a), relatively faster process resulted in a uniform thin layer (upper part) with a weak iridescent color while the slow evaporation produced a thick layer with many cracks (lower part), formed by volume shrinkage during drying. Fig. 2(b) represents the optical texture of a thick deposition. The texture reveals evenly thick layer with many cleavages in a wide area.

The FE-SEM images present detailed surface morphology of the SNPs-layer. The magnified FE-SEM micrograph in Fig. 2(c) corresponds to the upper uniform region in Fig. 2(a). It presents a close packing of the SNPs with no crystalline order, probably due to polydispersity of a particle size. On the other hand, a flat smooth but quite thick deposition with a wide crack was observed in the slow processed region as shown in Fig. 2(d). The magnified view of a surface in Fig. 2(e) is quite distinct from the surface in (c). Here the

Optics EXPRESS

packing of SNPs was less dense with embedded pores and consequently the surface became rougher than that in a thin densely packed area.

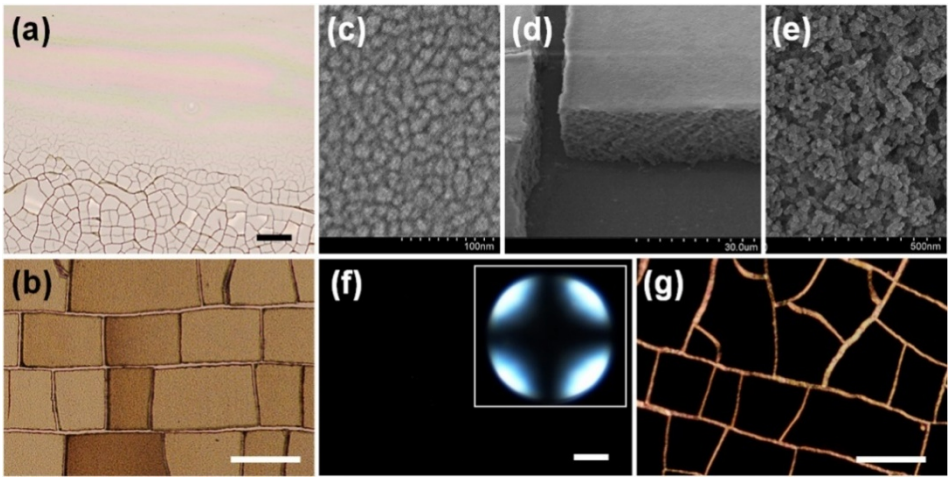

Fig. 2. Optical, scanning electron, and polarized optical micrographs of the multi-layered SNPs with an average 15 nm diameter: (a) Optical image of the silica layer formed by varied deposition rate; (b) Optical image of the thick deposition; FE-SEM visualizations of the (c) thin layer with a normal view, (d) thick layer with a tilted view, and (e) magnified normal view of the thick layer; POM and conoscopic images of the LC cells fabricated with (f) thin and (g) thick silica layers. Scale bars for optical images correspond to 10 μm. Bright lines in (g) correspond to the crack-lines in (b).

Although no crystalline nature of the packing was observed for both cases, LC molecules were aligned vertical to the substrate for both thin and thick regions as observed on the opal crystal. Fig. 2(f) demonstrates a uniform vertical alignment of the LC cell fabricated by employing thin layers of SNPs-deposition. The conoscopic Figure in the inset confirms a vertical orientation of the optic axis (i.e., nematic director). The thick deposition also induced homeotropic anchoring on the surface as seen in Fig. 2(g). Although a random planar alignment was evidenced by the bright lines in cracked areas with a bare ITO-surface, the horizontally leveled SNPs-surfaces promoted uniform vertical alignment.

The other example of irregular roughened surface of the SNPs-layer was prepared using polydisperse 80 nm SNPs. Optical, scanning electron, and polarized optical images of the SNPs-layer showed similar characteristics to those in Fig. 2. More detailed characterization on the surface was performed by AFM and results were presented in Fig. 3. Fig. 3(a) shows a surface topography of the bare ITO-substrate. 2D and 3D views present irregularity of the surface. The green plot shows a surface profile along the green line in 2D image. The average and RMS roughness were 0.25 nm and 0.32 nm, respectively. The histogram shows the height distribution of protrusions, showing a 1.4 nm of average height. Fig. 3(b) reveals a surface topography of the SNPs-layer. Much distinct roughness was observed in 2D/3D images and surface profile (green plot) by noting difference in the depth scale (z-axis). In this case, the average and RMS roughness were 22.4 nm and 28.9 nm, respectively. The histogram shows a 214.3 nm of average height of protrusions. The surface roughness of the SNPs-layer is approximately two orders of magnitude larger than that of a bare ITO-surface.

Electro-optical properties were characterized using the LC cells with Δnd ~300 nm. Fig. 4(a) shows measured transmittance as a function of applied voltage. Two types of LC cells were prepared using conventional PI-films (black circles) and 15 nm SNPs-layers (blue diamonds) as alignment layers. The inset corresponds to the POM images for the dark and bright states of the cell with the SNP-layers. The LC cell with SNPs responded to slightly lower threshold ($T_{10\%}$) voltage (2.2 V vs. 2.4 V) while the saturation ($T_{90\%}$) voltage of the

Optics EXPRESS

SNPs-cell was higher (4.0 V and 3.9 V). The discrepancies between the SNPs-cell and conventional PI-cell seems originating from the flow-induced pretilt of director on the SNPs-

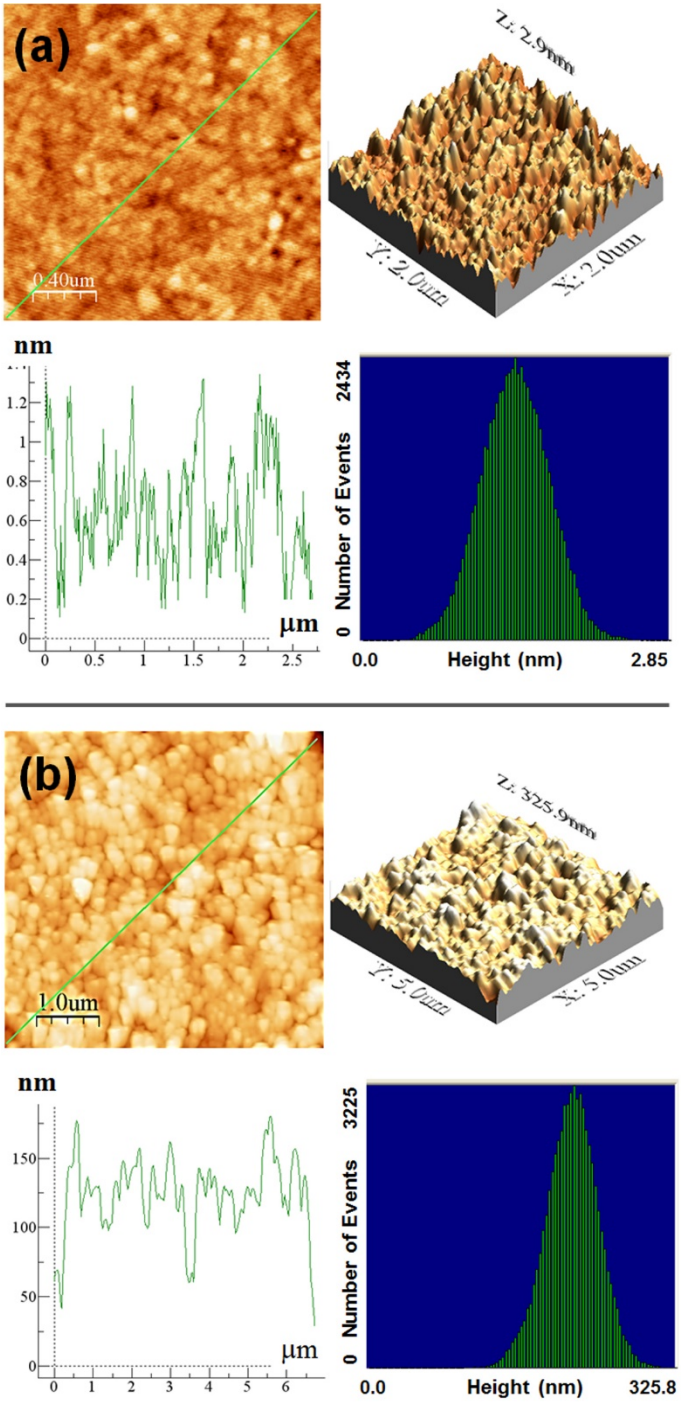

Fig. 3. Surface topographies of the (a) bare ITO-substrate and (b) thick silica layer, deposited using polydisperse 80 nm SNPs. The plots correspond to the surface profiles along the green diagonal lines in 2D-images. The histograms exhibit the number of events counted by the height of discrete aggregates.

Optics EXPRESS

surface. Otherwise, this could be attributed to the slight difference in cell gap rather than alignment layers.

Turn-on and -off time of the SNPs-cell were compared to those of the PI-cell. Turn-on (off) time was defined as the time taken for the transmittance to reach from $T_{10\%}$ ($T_{90\%}$) to $T_{90\%}$ ($T_{10\%}$) with 5.0 V applied voltage. The turn-off time was in a similar range; 12.2 ms and 13.0 ms for the SNPs- and PI-cell, respectively. However, significant difference in the turn-on time was observed for the SNP-cell (11.5 ms) and PI-cell (27.9 ms). It seemed that much faster turn-on response was attributed to the less populated transient defects, occurring during switching. In general, appearance of populated transient defects, caused by random fall-over of the LC director to the substrate plane, slows down the turn-on response time [21–23]. The

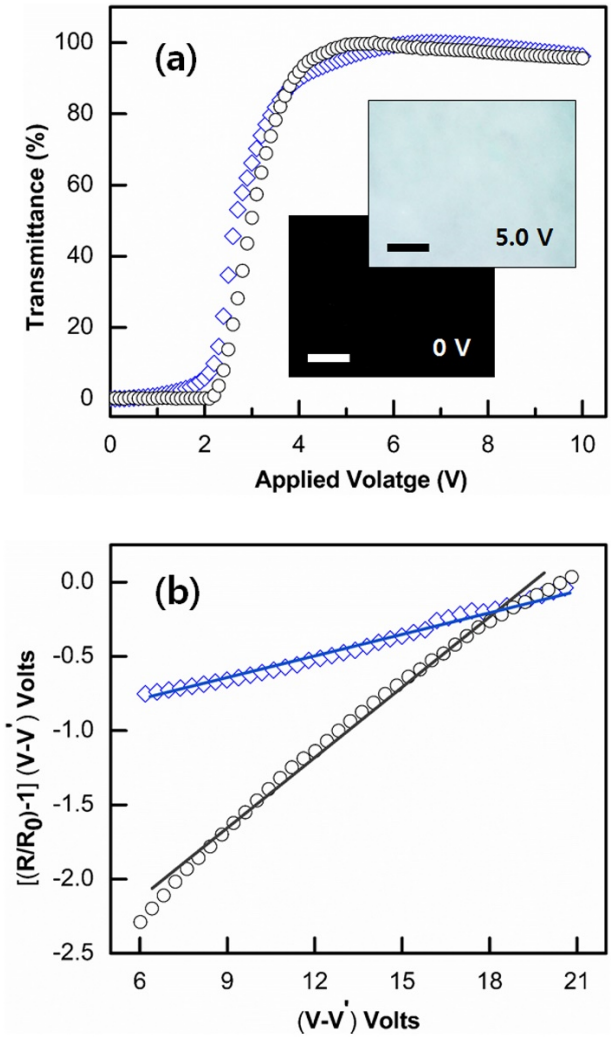

Fig. 4. Electro-optical switching characteristics and measured retardation values of the LC cells with 15 nm SNPs-layer (blue diamonds) and conventional PI-layer (black circles): (a) Voltage vs. Transmittance curves of the LC cells with different alignment layers, and (b) plots of measured (R/Ro–1) (V–V′) vs. (V–V′) used for the calculation of polar anchoring energy. The inset in (a) presents POM images of the dark and bright states for the SNPs-cell at the corresponding applied voltage. Scale bars correspond to 20 μm.

rougher homeotropic surface showed a tendency to form a less transient defect during switching even with no predetermined director pretilt [21–23].

Optics EXPRESS

In addition, the surface anchoring energy is an important parameter for a LC cell, as it affects not only the LC alignment but also the electro-optic properties. To evaluate anchoring strength of LC molecules on each surface, the retardation values of both SNPs-cell and PI-cell were measured, and plotted as in Fig. 4(b). The results showed a good linear fit for both SNPs-cell (blue diamonds) and PI-cell (black circles) in a high voltage region. The slope of linear fitted line was used to calculate polar anchoring energy of LC molecules on each surface. The resulting polar anchoring energy on SNPs- and PI-surface was found to be 5.51 $\times$ 10^{-5} J/m^2 and 2.11 $\times$ 10^{-5} J/m^2, respectively. This result demonstrates that anchoring strength of the SNPs-layer is stronger than that of the conventional PI used as reference and therefore is sufficiently strong for device applications.

In general, LC alignment on a solid surface is understood either by chemical [3,17,44,45] or physical [19,20,42] interactions between LC molecules and the surface. Anchoring of LC molecules on a smooth amorphous solid surface is mostly known as random planar alignment (i.e., tangential anchoring of long molecular axis to a surface with no in-plane order), which maximizes van der Waals interaction between a LC and surface. When the surface consists of oriented chemical segments, however, a LC director aligns specifically with respect to the anisotropic segments (i.e., chemical interaction determined by chemical components). If the surface is composed of amorphous solid with a grooved structure, a LC director aligns parallel to the groove [40–42]. The grooved surface with a planar anchoring enhances elastic deformation of LCs in the bulk to a great extent if the director aligns transverse to the groove. In this case, the LC director preferably aligns parallel to the groove to avoid elastic deformation although the surface has no chemical anisotropy (i.e., physical interaction) [40–42]. For the same reason, anchoring transition from a planar to homeotropic state spontaneously occurs when LC molecules are placed on a two-dimensional grooved surface. Because the LC director in any direction in the surface plane induces high elastic deformation of LCs, the director escapes to the third dimension (i.e., normal to the surface) [40,41].

Homeotropic alignment of LCs on the opal crystal can be explained in the same context by the Berreman's model [20]. The anchoring of LCs on a smooth untreated silica surface is generally known as a planar state [46,47]. The physical interaction concentrates on elastic energy of bulk LCs while the chemical interaction focuses on the coupling, mainly through vander Waals interaction, between a surface and LC molecule. Ultimately LC alignment is determined by the competition between the chemical and physical interactions to minimize a total free energy of the system. Therefore, the competition between the chemical anchoring strength on a flat smooth surface and elastic deformation of LCs caused by an uneven surface should be considered to understand the anchoring transition of LC alignment at different surface topographies. If chemical anchoring is strong enough to overwhelm elastic deformation, LCs will align preferable to the chemical interactions, yielding tangential anchoring to the surface. However, LC alignment will favor the physical interaction to minimize elastic free energy when elastic deformation energy predominates chemical anchoring energy.

Figs. 5(a) and 5(b) schematically illustrate a planar and homeotropic LC alignment at the surface of closely packed SNPs [40–42]. The LC anchoring depends on competition between surface anchoring energy (W_a) and bulk elastic energy (W_e) of the system. As shown in Fig. 5(a) for a planar anchoring, elastic deformation of LCs critically depends on the amplitude-frequency ratio (a/λ). If a/λ << 1, the elastic deformation is comparatively weaker than the chemical anchoring. Therefore LC molecules prefer to align tangential to the surface of SNPs. If a/λ >> 1, however, the chemical anchoring energy is overwhelmed by the elastic energy. As a result, LC molecules favor homeotropic anchoring as shown in Fig. 5(b).

Optics EXPRESS

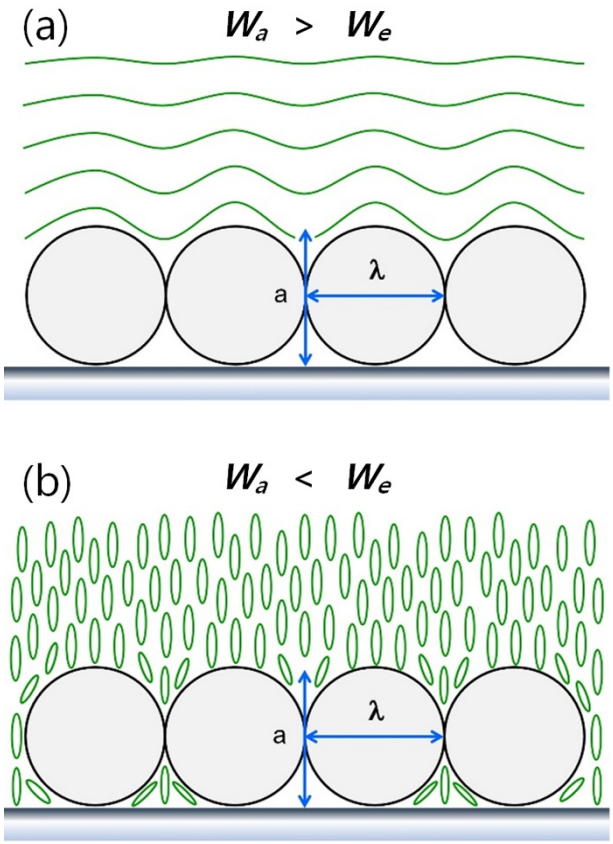

Fig. 5. Schematic illustration of LC alignment at the surface of closely packed nanoparticles. The green solid lines in (a) depict tangential direction of a local LC director. The green ellipse in (b) represents LC molecule. W_a and W_e denote anchoring energy and elastic energy of LCs, respectively.

For the monolayer of spherical particles (i.e., 2D opal crystal), the a/λ = 1 and LC anchoring depends on the size of particles. If the chemical anchoring is infinitely strong, the director is aligned tangential to the surface of SNPs despite of elastic deformation of LCs. For finite anchoring strength, however, the critical diameter d of SNPs for anchoring transition can be approximated by the estimation on typical anchoring energy at ordinary surfaces and elastic constant of LC material. The polar anchoring energy of smooth solid surfaces ranges $W_a \sim 10^{-5}$ J/m. The elastic constant of LCs is in the order of $K \sim 10^{-11}$ N. In this case, the anchoring scale, which is defined as the critical length for the anchoring transition from a planar to homeotropic state, is $L_w = K/W_a \approx 10^{-6}$ m = ~1 μm for the chemical interaction to a smooth surface [48]. Similarly for the 2D-grooved surface with a frequency λ and amplitude a, approximate anchoring energy [40] is $W_a \sim Ka^2/\lambda^3$ and the measured polar anchoring energy was in the order of $W_a \sim 10^{-5}$ N/m in the present experiment. Thus the anchoring scale $L_w = K/W_a \sim \lambda^3/a^2 = \sim 1$ μm.

The anchoring scale based on both chemical and physical interactions suggests that a critical length scale for the anchoring transition from a planar to homeotropic state is ~1 μm. If a diameter $d >> 1$ μm, anchoring energy contribution to the total free energy is dominant over elastic free energy and thus LC anchors planar to a surface. On the contrary, for the $d << 1$ μm, LC director aligns vertical to the surface. The estimation is valid for particles with various chemical compositions with polar anchoring energy $W_a \sim 10^{-5}$ N/m. According to the discussion, Fig. 5(a) illustrates a planar anchoring condition, where $\lambda^3/a^2 >> 1$μm representing

Optics EXPRESS

$W_a >> W_e$. Contrariwise, when $\lambda^3/a^2 << 1$ μm, LCs anchor vertical to the surface as illustrated in Fig. 5(b), where elastic energy dominates anchoring energy (i.e., $W_a << W_e$).

Based on our results with polydisperse SNPs, roughness of a surface is a critical parameter for a homeotropic alignment rather than regularity of protruded surface. For the flat surface with closely packed small particles with d (diameter) ~l (molecular length), the surface may not be rough enough to induce elastic deformation of LCs. This doesn't mean that the particles with d ~l are not able to induce homeotropic alignment. The SNP-layers composed of irregular clusters of primary aggregates can form a rough enough surface with embedded pores similarly as in Fig. 2. In this case, the anchoring energy W_a depends on the average amplitude-to-frequency ratio of protrusions (A/Λ). Here A is the average amplitude of the protrusions and Λ is the average of spatial periodicity (frequency). Consequently, critical length scale for anchoring transition can be approximated by $L_w = K/W_a \sim \Lambda^3/A^2 = \sim 1$ μm. If $\Lambda^3/A^2 << \sim 1$ μm, the elastic deformation of a bulk LC overwhelms the anchoring energy at the surface and thus leads anchoring transition to a vertical alignment.

4. Conclusion

In this work, homeotropic alignment of LCs on the SNPs-depositions has been demonstrated. Self-assembled opal crystals were deposited on flat substrates by the capillary convection method and used as LC alignment layers. The SNPs-layers with regular or irregular protruded surface induced vertical alignment of LC director with respect to a surface plane. Compared to the conventional PI-cell, the SNPs-cells showed sufficient optical, electro-optical, and anchoring properties for device applications.

The origin of homeotropic anchoring of LC molecules on the opal crystal is physical in nature. The results corroborate the model of physical interaction first proposed by Berreman. For polar anchoring of LC molecules on the surface of SNPs-layer, topography (i.e., roughness) plays a crucial role rather than chemical composition of nanoparticles or regularity of the surface. Approximate estimation resulted the critical length scale $L_w = \sim 1$ μm for anchoring transition. If a diameter of particle $d << 1$ μm for a 2D opal crystal, LC molecules prefer to anchor vertically to the surface to minimize elastic free energy of bulk LCs. For the SNPs-layers composed of irregular clusters of primary aggregates, LC anchoring is determined by the average amplitude-to-frequency ratio of protrusions (A/Λ). If $L_w = \Lambda^3 A^2 << \sim 1$ μm, the elastic deformation of a bulk LC governs the anchoring at the surface and thus leads to homeotropic alignment. The results and discussion provide crucial intuition regarding the LC-anchoring on a solid surface. This suggests that homeotropic alignment of LCs can be achieved by various unconventional approaches, making rough surfaces instead of forming a conventional polymer layer.

Funding

BK21 Plus Project through the National Research Foundation of Korea.

Disclosures

The authors declare that there are no conflicts of interest related to this article.